ENHANCING UAV-SfM 3D MODELS ACCURACY OF UNIQUE HERITAGE INFRASTRUCTURES. CASE OF ISABEL II DAM, ALMERIA, SPAIN

F. Agüera-Vega[1,2] *, P. Martínez-Carricondo[1,2], F. Carvajal-Ramírez[1,2]

[1] Escuela Superior de Ingeniería, Universidad de Almería, 04120, Almería, Spain - (faguera, pmartinez, carvajal)@ual.es
[2] Centro de Investigación Mediterráneo de Economía y Desarrollo Sostenible, Universidad de Almería, 04120, Almería, Spain

KEY WORDS: UAV, Photogrammetry, Points Cloud, Infrastructure Heritage, structure-from-motion photogrammetry.

ABSTRACT:

In recent years, resources and computer tools have devolved to allow the production of three-dimensional (3D) models that have become great sources of data for the reconstruction of elements of forgotten heritage. The main advances in the field of 3D modelling are related to terrestrial laser scanning (TLS) and unmanned aerial vehicle (UAV) photogrammetry. Thanks to the development of image processing techniques, such as structure from motion (SfM) and multiview stereopsis (MVS), combination of both techniques offers effective and cost-efficient photogrammetric process to obtain a high-resolution data set from photographs taken from different points of view. The goal of this paper is to study the effect of the number and distribution of GCP, and the inclusion of oblique photographs on the accuracy of the 3D points clouds yielded by UAV photogrammetry. To achieve this purpose, 18 UAV photogrammetric projects, combining number and distribution of GCPs and inclusion of oblique images to the nadir images, were developed, and the accuracy, precision, and distance respect to a reference cloud were estimated. Results concluded that when only nadir images are used, the best results were found with nine GCPs placed at each of the four corners of the object under study, four in the midpoint of each line that joins two consecutive corners, and another one in the midpoint. Maintaining this arrangement of GCP and adding 12% of oblique images with respect to the total of zenith images, with an angle of 20º with respect to the nadir, improves the precision of the 3D point cloud generated by the photogrammetric project. If it is not possible to place the GCPs in this arrangement, the best option is to place them at the top of the dam.

1. INTRODUCTION

Unmanned aerial vehicles (UAVs) are widely used platforms to provide high temporal and geometrical resolution data for mapping and modelling for geosciences and engineering purposes (Carricondo et al., 2021; Carvajal-Ramírez et al., 2019; Ferrer-González et al., 2020; Gong et al., 2019; Mancini et al., 2013; Menegoni et al., 2020; Mourato et al., 2017; Rossi et al., 2018). A wide range of sensors can be attached to a UAV, although the most commonly used for mapping purposes are digital cameras, which despite not being metric, have a lightweight and high image quality (Manconi et al., 2019). Furthermore, due to the development of image processing techniques, such as structure from motion (SfM) and multiview stereopsis (MVS), combination of UAVs, SfM and MVS (for the sake of simplicity, this combination will hereafter be referred to as UAV-SfM) offers effective and cost-efficient photogrammetric techniques to obtain a high-resolution data set (Westoby et al., 2012). SfM technique provides a sparse 3D point cloud in an arbitrary coordinate system and a full camera calibration, solving the collinearity equations without the need for any ground control point (Fonstad et al., 2013; Pérez et al., 2011). This is possible due to image matching algorithms that automatically search for similar image objects (key points) by analysing the correspondence, similarity and consistency of the image features (Ao et al., 2018). SfM paired with MVS yield a dense 3D point cloud (Furukawa & Ponce, 2010).

When the object under study has a complex geometry, it is necessary to pay special attention to the image capture and processing techniques to obtain reliable results (reduce data gaps and obtain high accuracy and precision) in planimetric and altimetric dimensions. Some of the main considerations in flight planning for UAV-SfM are the flight altitude, camera axis angle regarding the object, and the front and side overlap. Together with the sensor dimension, resolution, and focal length, all of these parameters determine the ground sample distance (GSD) and the accuracy and precision of the final results (Manconi et al., 2019). A combination of nadir and oblique images can produce a more precise self-calibrating bundle adjustment when using nadir images alone due to better internal calibration of the camera (James and Robson 2014; Harwin et al. 2015), which largely determines the accuracy of photogrammetric products.
In this regard, (Stroner et al. 2021) and (Bi et al. 2021) observed an improvement in the vertical accuracy of UAV photogrammetric project products using GNSS RTK techniques by including oblique images. Furthermore, the final accuracy of the 3D point cloud produced by the photogrammetric project, as well as the validity of the comparison of clouds generated at different times or from different sensors, is conditioned by the georeferencing strategy and the number and distribution of GCPs. Temporal analysis of objects morphology requires high accuracy of measurements and reproducibility of the methodology as differencing of digital surface models leads to error propagation. In Clapuyt et al. (2016), a study area characterized by gently topography was surveyed with a UAV platform equipped with a standard reflex camera, varying the focal length of the lens and location of GCPs between flights. They concluded that the survey accuracy and distribution of GCPs play an important role in preventing changes detected on a surface measured at different times from being due to the error made in measuring the GCPs.

* Corresponding author

In view of the above, it is necessary to deepen the knowledge of the influence that certain factors related to the planning of the photogrammetric flight, such as image angle, or the GCPs number and distribution, have on the quality of the 3D point cloud obtained from the photogrammetric projects derived from the flights.

The goal of this paper is to study the effect of the number and distribution of GCP, and the inclusion of oblique photographs on the accuracy of the 3D points clouds yielded by UAV photogrammetry. The conclusions will give a set of tips to take into account for infrastructure heritage UAV photogrammetry.

2. MATERIAL AND METHOD

To achieve the proposed objective, nine GCPs were sprayed over the study site and three flights were conducted, one with nadir camera angle and two with not nadir camera angle. By combining photographs of the different flights and combinations of GCPs, 18 UAV-SfM photogrammetric projects were derived. Furthermore, a 3D point cloud was collected with a terrestrial laser scanner (TLS). All these 3D point clouds were georeferenced using the same set of GCPs. With the TLS reference cloud, distance between this and each of those derived from the UAV-SfM projects calculated in every point allowed to have an error distribution on the whole study site and to derive mean and standard deviation statistics.

2.1 Study Site

This research focused on the Isabel II Reservoir, located in south-eastern Spain, in the province of Almería and a few kilometres from the village of Níjar (Fig. 1). It consists of several elements, such as the body of the dam, which is the study object, the administration building, the control tower or the irrigation distribution canals.

The dam, built in the nineteenth century, stands out as one of the most spectacular elements of Spanish structural and hydraulic heritage. It is also a world reference for arch-gravity dams built in stone (García-Sánchez, 2014). It is approximately 35 m high and 44 m long; limestone ashlar stones were used for the exterior surfaces and lime masonry for the interior (Fig. 2).

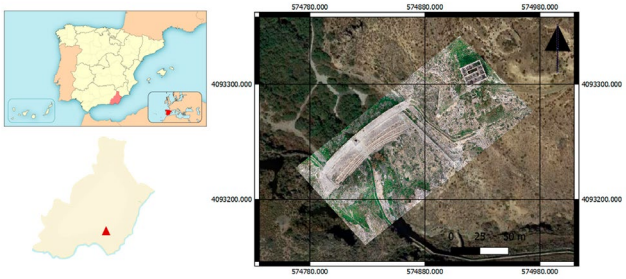

Figure 1. Location of the dam.

Figure 2. Perspective of the study object.

2.2 Ground Control Points measurement

Un total de nueve GCPs distribuidos por toda la presa fueron medidos mediante técnicas GNSS. Aprovechando que la presa tiene forma de escalera, se dispusieron tres GCP en la zona más alta de la misma, tres en una zona algo más baja y otros tres más abajo. En cada nivel, dos GCPs se dispusieron en los extremos de la presa y el tercero en la zona central (Fig. 3).

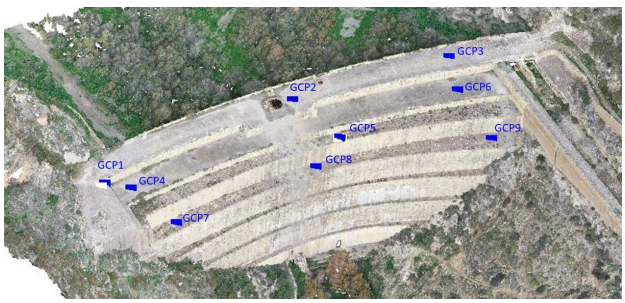

Figure 3. Ground Control Points location.

The GCPs were materialized by means of targets that allowed for their later viewing in the aerial photographs. These targets consisted of a red paper of A3 size (420x297 mm) with four quadrants, two of them black. The three-dimensional (3D) coordinates of these targets were measured with a GNSS receiver operating in post-processing kinematic mode (PPK), with the base emitting corrections at a point near the dam. Both rover and base GNSS receivers were Trimble R6 systems. The 3D coordinates of the base, corrected via the Trimble Centerpoint RTX Post-Processing Service, were 574909.418, 4093250.721, and 372.012 m (European Terrestrial Reference System 1989)

2.3 TLS 3D points cloud reference

Trimble TX8 Scanner was utilized for the topographical survey of the dam. This scanner measures almost 1 million points per second and its maximum scanning range is 120 m. Due to the geometry of the study area, it was not possible to capture the entire dam from a single TLS location. Therefore, the measurements for the TLS point cloud acquisition were taken from four different station locations. Processing of the point clouds obtained by TLS was carried out using Trimble RealWorks software, resulting in a final TLS point cloud by combining the four individual point clouds. To reduce the size of the resulting point cloud, limits were established according to the area of interest, resulting in a point cloud of 74,447,399 points, from which a cloud of 710729 points was derived by random extraction. This reduced cloud was used to make

comparisons with the clouds derived from the photogrammetric projects performed.

2.4 UAV image capture and processing

The images were captured by a rotary wing with four rotors, DJI Phantom 4 Pro UAV. This equipment has a navigation system that uses GPS and GLONASS constellations. Its RGB camera is equipped with a one-inch, 20-megapixel (5472 x 3648) sensor and has a manually adjustable aperture (from F2.8 to F11). The lens has a fixed focal length of 8.8mm and a horizontal field of view (HFOV) of 84º.

The images were obtained from three independent flights. The first was carried out in automatic pilot mode through the DJI GS Pro application, and a total of 151 nadir photographs were obtained in 13 passes. The flight height was set at 36 m above the dam crest, which is equivalent to a ground sample distance (GSD) of 1.3 cm. To obtain side and forward overlaps of 65% and 80%, respectively, the camera took a shot every two seconds. The second flight was made in manual mode to obtain oblique photographs, to provide photographic capture of all the details of the dam´s geometry. This flight was carried out at an approximate distance of 5 m from the downstream face of the dam and was executed in one passe, parallel to the dam, at 30 m above the dam crest, with a camera angle of 20º respect to nadir angle. A total of 18 images were taken in this flight. The third flight was made in manual mode too, with two passes at different flight heights, one at the same height of dam crest and one 10 m bellow the dam crest, both at an approximate distance of 20 m from the downstream face of the dam. The camera angle was 65º respect to nadir angle. A total of 51 images were taken. Figure 4 shows the location of each photograph taken on each of the flights described above.

The images were processed using Pix4Dmapper, version 4.6.4, commercial software, which incorporates an algorithm based on SfM-MSV techniques. The complete workflow includes several processes, which can be divided into the following three main steps: 1. Initial Processing, 2. Point Cloud and Mesh, and 3. DSM, Orthomosaic and Index., but this study used only the dense 3D points cloud. One process included in the first step is a self-calibrating bundle adjustment based on camera internal and external orientation parameters. The photogrammetric projects were processed using the setting shown in Table 1.

To avoid the influence of the marking of the GCPs between the different projects on the results, this marking was performed on a general project that included all the GCPs and the photographs corresponding to the three flights performed. From this, the photographs and GCPs used in each of the different projects studied were fixed by deactivating those that did not belong to the project studied at that time.

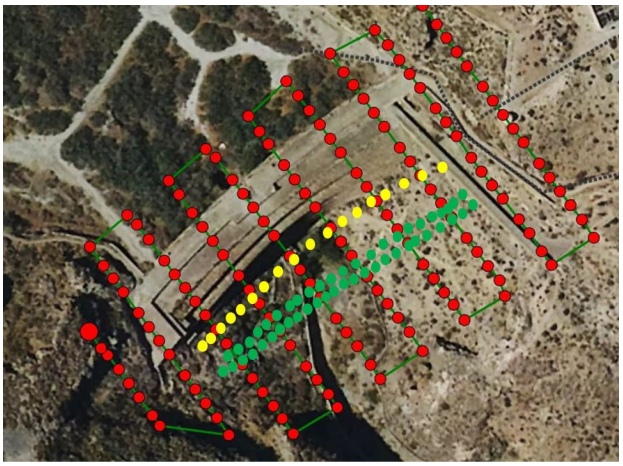

Figure 4. Location of each photograph taken on each of the flights. Red points correspond to the nadir flight, yellow points correspond to 20º flight, and green points correspond to 65º flight.

Pix4Dmapper Step	Processing Option	Setting
1. Initial project processing	General/Keypoint Image Scale	Full
	Matching/Matching Image Pairs	Aerial Grid o Corridor
	Calibration/TargetedNumber of Keypoints	Method: Standard Automatic Standard
	Calibration/Calibration	ll Internal and External Parameters Optimization
	Calibration/Rematch	Rematch: Automatic
	Calibration/Export	Automatic Camera Internals and Externals, AAT, BBA .AT: automatic aerial triangulation; BBA: bundle block adjustment)
2. Point cloud and mesh	Point Cloud/Image Scale	½ (Half image size, Default)/
	Point Cloud/Point Density	Multiscale Optimal
	Point Cloud/Minimum Number of Matches	3
	Advanced/Matching Window Size	7x7 pixels

Table 1. Setting of processing options in Pix4Dmapper for all processed photogrammetric projects.

Combinations of flights and GCPs resulted in 18 different photogrammetric projects, as shown in table 2.

Project	images	GCPs used
01-NADIR	Nadir images	1, 2, 3, 4, 5, 6, 7, 8, 9
02-NADIR	Nadir images	1, 2, 3
03-NADIR	Nadir images	4, 5, 6
04-NADIR	Nadir images	7, 8, 9
05-NADIR	Nadir images	1, 3, 5, 7, 9
06-NADIR	Nadir images	1, 3, 7, 9
01-OBLIQ1	Nadir + 20º images	1, 2, 3, 4, 5, 6, 7, 8, 9
02-OBLIQ1	Nadir + 20º images	1, 2, 3
03-OBLIQ1	Nadir + 20º images	4, 5, 6
04-OBLIQ1	Nadir + 20º images	7, 8, 9
05-OBLIQ1	Nadir + 20º images	1, 3, 5, 7, 9
06-OBLIQ1	Nadir + 20º images	1, 3, 7, 9
01-OBLIQ2	Nadir + 65º images	1, 2, 3, 4, 5, 6, 7, 8, 9
02-OBLIQ2	Nadir + 65º images	1, 2, 3
03-OBLIQ2	Nadir + 65º images	4, 5, 6
04-OBLIQ2	Nadir + 65º images	7, 8, 9
05-OBLIQ2	Nadir + 65º images	1, 3, 5, 7, 9
06-OBLIQ2	Nadir + 65º images	1, 3, 7, 9

Table 2. Combination of photographs and GCPs used in each of the 18 photogrammetric projects studied.

2.5 Accuracy assessment

In order to assess the accuracy of the 3D point clouds generated from each studied photogrammetric project, the freely available Multiscale Model to Model Cloud Comparation (M3C2) algorithm was used (Lague et al., 2013). It is offered as a plugin by the CloudCompare software (https://www.danielgm.net/cc/, accessed 26 April 2023). The M3C2 algorithm calculates the local differences between the reference cloud (described in the 2.3 section) and the compared point cloud (those derived from the photogrammetric projects) relative to a local surface normal orientation following two different steps. The first step describes a user-defined diameter (called normal scale, D) that is used to calculate the normal orientation in the reference cloud. All points included in a sphere of diameter D and centre in the point under study are used to fit a plane, which defines the normal orientation. In the second step, a second user-defined diameter (called projection scale, d) is used to define a cylinder with diameter d and axis parallel to normal orientation, including the point under study. Furthermore, the height of the cylinder is defined (h). All points of both clouds are projected on the cylinder axis, giving two distributions of distances, with origins on the point under study. The mean of each distribution gives the average position of each cloud along the normal direction, and the standard deviations provide a local estimate of the point cloud roughness. The local distance between the two clouds is given by the distance between the two calculated means.

From all calculated local differences, a distribution function of the local differences can be obtained, and their mean value and standard deviation can be calculated. This was done for each of the clouds generated in each of the 18 photogrammetric projects. On the one hand, the absolute value of the mean difference can be assimilated to the accuracy of the photogrammetric project 3D points cloud, where the values closest to zero for this difference indicates better accuracy, and on the other hand, the standard deviation can be assimilated to the precision of the photogrammetric project 3D points cloud. The normal scale (D) was set as 25 times the average local roughness calculated for the reference cloud by CloudCompare (D = 0.25 m) to ensure that the normal direction is unaffected by point cloud roughness. In addition, the projection scale was set to d = 0.15 m, and the height of the cylinder was set to h = 1m.

3. RESULTS AND DISCUSSION

Figures 5 and 6 show the M3C2 absolute mean distance (accuracy), and the standard deviation (precision), respectively, calculated from the distances measured between the reference 3D points cloud and the 3D points cloud yielded by each UAV photogrammetric project. As can be seen in Figure 5, the accuracy presented worse values in the OBLIQ2 projects than in the NADIR and OBLIQ1 projects, regardless of the set of GCPs considered, except for project 04OBLIQ2, where it was worth 0.0025 m, which represented the best accuracy. The difference between the NADIR and OBLIQ1 projects was small, although the OBLIQ1 projects showed better values than the NADIR projects, except for the GCP 06 combination (0.0174 m vs. 0.0166 m). Accuracies yielded by GCPs combination 01, 05 and 06, for NADIR and OBLIQ1 projects, were quite similar, but in the NADIR and OBLIQ1 projects, the minimum accuracy values were found for the GCP 02 combination: 0.0064 m and 0.0061, respectively.

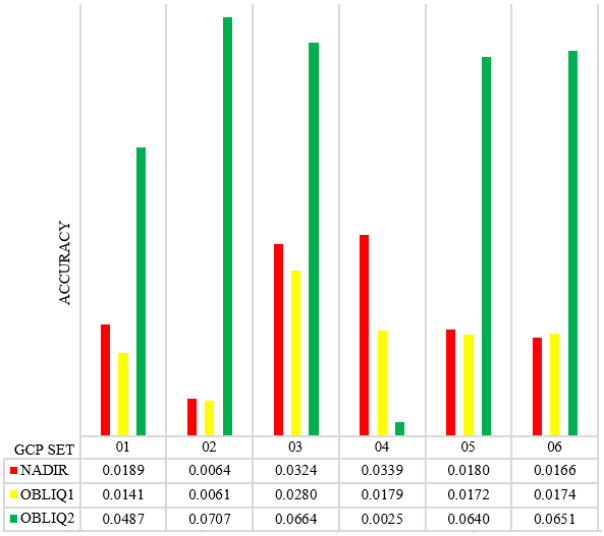

GCP SET	01	02	03	04	05	06
NADIR	0.0189	0.0064	0.0324	0.0339	0.0180	0.0166
OBLIQ1	0.0141	0.0061	0.0280	0.0179	0.0172	0.0174
OBLIQ2	0.0487	0.0707	0.0664	0.0025	0.0640	0.0651

Figure 5. Accuracy (M3C2 absolute mean distance), calculated from the distances measured between the reference 3D points cloud and the 3D points cloud yielded by each photogrammetric project.

The precisions represented in Figure 6 show a similar trend as the accuracy for the OBLIQ2 projects: the values were worse than in the NADIR and OBLIQ1 projects. The 04OBLIQ2 project, which produced the best accuracy value, presented the worst precision value (0.10235 m) of all the projects studied. Contrary to what was observed for accuracy, precision always presented the best values in OBLIQ1 projects, regardless of the GCP combination considered. The best precision was yielded by the project 01OBLIQ1 (0.03396 m). Considering both precision and accuracy, there is no project that presents the best values of both. For example, as just indicated, project 04OBLIQ2 presented the best value for accuracy but also presented the worst value for precision. Project 01OBLIQ1 produced the best precision value, 0.03396 m, while the accuracy of the same project was 0.0141 m, which although not the best value, is in the group of the best.

This indicates that when designing a photogrammetric project for the type of objects studied in this work, a compromise solution must be reached to optimize both the precision and accuracy of the generated 3D point cloud.

In view of data presented in figures 5 and 6, an adequate design of photogrammetric project could be composed by a combination of nadir images and a set of oblique images taken at approximately 20º respect to the nadir orientation, and a set of nine GCPs, with one in the middle of the study area and the rest distributed along the study area contour. Among the studied projects, the 01OBLIQ1, is the optimum: 0.0141 m accuracy and 0.03396 m precision. In (Agüera-Vega et al., 2022) found improvement of accuracy and precision when a set of 20º oblique images were combined with nadir images, in UAV photogrammetric projects of complex morphology terrains.

Similar results were reported by (Nesbit & Hugenholtz, 2019), although they report bigger angles, between 20º and 35º, for reaching this improvement. Previous works suggested that oblique images should account for approximately 10% of the nadir images (e.g. Carbonneau and Dietrich 2017; Nesbit and Hugenholtz 2019) as a higher proportion means poorer results.

GCP SET	01	02	03	04	05	06
NADIR	0.05155	0.05338	0.04846	0.10235	0.06058	0.06136
OBLIQ1	0.03396	0.04213	0.04005	0.08747	0.04625	0.04609
OBLIQ2	0.08111	0.09998	0.08772	0.10375	0.05175	0.0526

Figure 6. Precision (M3C2 standard deviation distance), calculated from the distances measured between the reference 3D points cloud and the 3D points cloud yielded by each photogrammetric project.

In our work, oblique images represent 12% in OBLIQ1 projects, and 34% in OBLIQ2 projects. The results found in the OBLIQ1 and OBLIQ2 projects agree with the previous statement, although the number of images added to the set of nadir images and the angle at which they were taken must also be taken into account, since there are previous works which report its influence on the quality of the generated 3D point cloud. In our work, worse accuracy and precision values were generally found when the imaged angle increased. Nevertheless (Stroner et al. 2021) combined vertical images with images with an angle of 15º on one side and a 30º on the other, obtaining the best results (worst systematic error not exceeding 0.03 m) in the second case. The research by (Bi et al. 2021) covered the study area with vertical images and added 45º angled images taken from the last waypoint of the initial route to the centre of the study area. They concluded that by adding a small number of oblique images the elevation accuracy improved significantly. In any case, the larger angle used in our work was greater than any of those used in the aforementioned works, even the horizon appearing in some of the images used, which may have a negative influence on the quality of the 3D point cloud.

Regarding the number of GCPs, the results show that optimal precision and accuracy values can be achieved by placing one GCP at each of the four corners of the object under study, four in the midpoint of each line that joins two consecutive corners, and another one in the midpoint.

Another important aspect related to the 3D cloud point quality is the spatial error distribution, as there are works which report systematics error influenced by the photogrammetric project design. Figure 7 shows the spatial distribution of M3C2-calculated distances between cloud reference and the cloud derived from each photogrammetric project. This figure shows that there is a general trend that concentrates the positive values of distances in the lower part of the dam, while the negative values tend to be concentrated in the upper part. This trend is more notable for 04 NADIR, 04OBLIQ1, and 04OBLIQ2 projects. Furthermore, projects 04, 05 and 06 show a concentration of positive distances in the vertical zones of the dam. Project 01OBLIQ1, which was the optimum for accuracy and precision values, is also the one with most uniform distribution of distances over its entire surface area, four in the midpoint of each line that joins two consecutive corners, and another one in the midpoint.

4. CONCLUSIONS

Planning UAV-SfM projects in objects with complicated geometry requires several considerations. Although not the best option, many UAV-SfM projects are planned with nadir imagery. In this case, optimal precision and accuracy values can be achieved by placing one GCP at each of the four corners of the object under study, four in the midpoint of each line that joins two consecutive corners, and another one in the midpoint.

Maintaining this arrangement of GCP and adding 12% of oblique images with respect to the total of zenith images, with an angle of 20º with respect to the zenith, improves the precision of the 3D point cloud generated by the photogrammetric project.

If it is not possible to place the GCPs in this arrangement, the best option is to place them at the top of the dam.

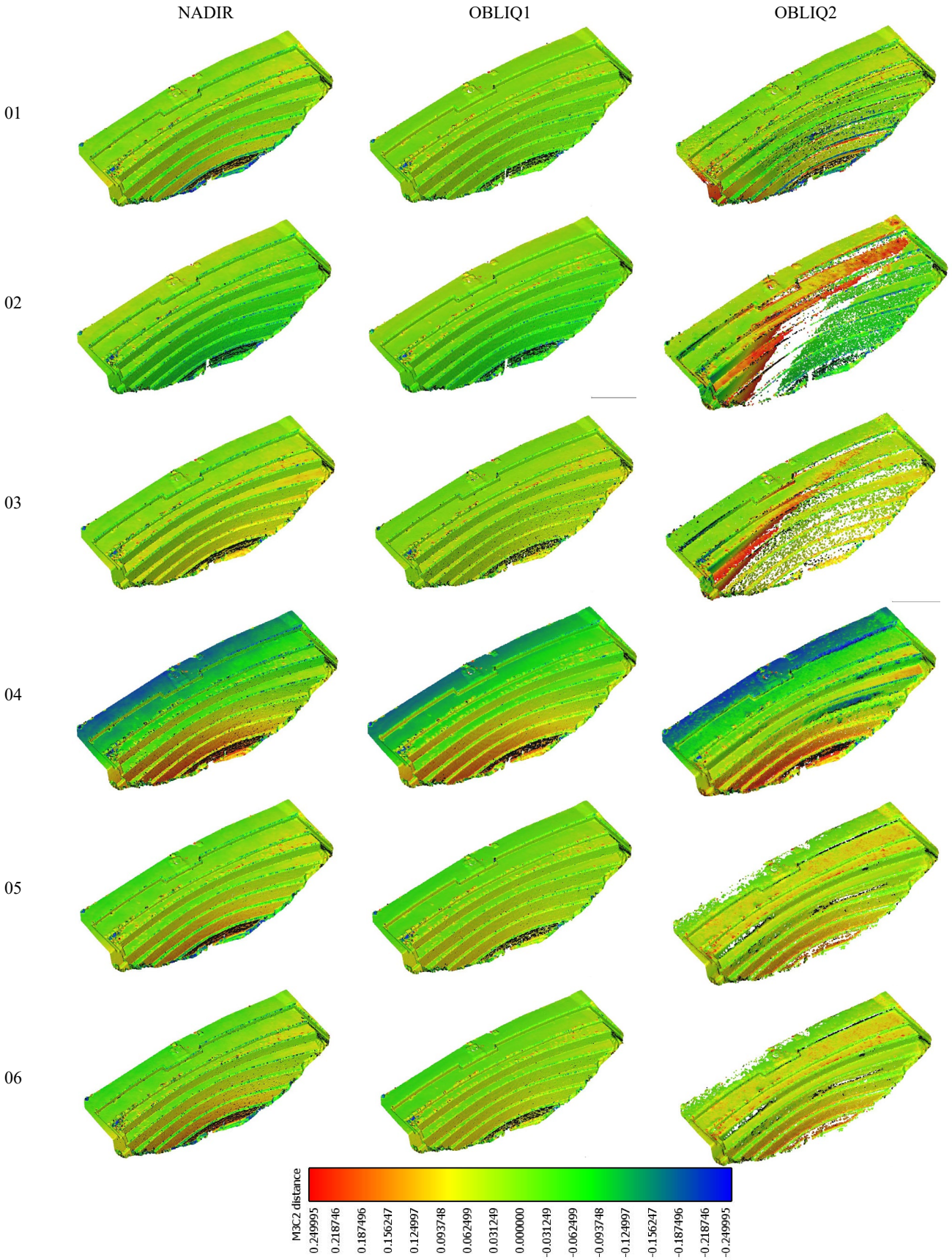

Figure 7. M3C2-calculated distances, in meters, between TLS reference cloud and clouds obtained from projects studied in this work. The top row indicates the type of project in terms of the angle of the images used. NADIR: 151 vertical images, OBLIQ1: 151 vertical images and 18 images tilted 20º with respect to nadir, OBLIQ2: 151 vertical images and 51 images tilted 65º with respect to nadir. The left column indicates the number and distribution of GCPs used in each photogrammetric project. See Table 2.

REFERENCES

Agüera-Vega, F., Ferrer-González, E., Carvajal-Ramírez, F., Martínez-Carricondo, P., Rossi, P., & Mancini, F. (2022). Influence of AGL flight and off-nadir images on UAV-SfM accuracy in complex morphology terrains. *Geocarto International*, *37*(26), 12892–12912. https://doi.org/10.1080/10106049.2022.2074147

Ao, T., Liu, X., Ren, Y., Luo, R., & Xi, J. (2018). An approach to scene matching algorithm for UAV autonomous navigation. *2018 Chinese Control And Decision Conference (CCDC)*, 996–1001. https://doi.org/10.1109/CCDC.2018.8407275

Carricondo, M., Sci, H., Carricondo-Martínez, P., Carvajal-Ramírez, Fernando Yero-Paneque, L., & Agüera-Vega, F. (2021). Combination of HBIM and UAV photogrammetry for modelling and documentation of forgotten heritage . Case study : Isabel II dam in Níjar (Almería , Spain). *Heritage Science*, 1–15. https://doi.org/10.1186/s40494-021-00571-8

Carvajal-Ramírez, F., da Silva, J. R. M., Agüera-Vega, F., Martínez-Carricondo, P., Serrano, J., & Moral, F. J. (2019). Evaluation of fire severity indices based on pre- and post-fire multispectral imagery sensed from UAV. *Remote Sensing*, *11*(9). https://doi.org/10.3390/rs11090993

Ferrer-González, E., Agüera-Vega, F., Carvajal-Ramírez, F., & Martínez-Carricondo, P. (2020). UAV photogrammetry accuracy assessment for corridor mapping based on the number and distribution of ground control points. *Remote Sensing*, *12*(15). https://doi.org/10.3390/RS12152447

Fonstad, M. A., Dietrich, J. T., Courville, B. C., Jensen, J. L., & Carbonneau, P. E. (2013). Topographic structure from motion: a new development in photogrammetric measurement. *Earth Surface Processes and Landforms*, *38*(4), 421–430. https://doi.org/10.1002/esp.3366

Furukawa, Y., & Ponce, J. (2010). Accurate, dense, and robust multiview stereopsis. *IEEE Transactions on Pattern Analysis and Machine Intelligence*, *32*(8), 1362–1376. https://doi.org/10.1109/TPAMI.2009.161

García-Sánchez, J. F. (2014). *El pantano de Isabel II de Níjar (Almería): paisaje, fondo y figura.*

Gong, C., Lei, S., Bian, Z., Liu, Y., Zhang, Z., & Cheng, W. (2019). Analysis of the Development of an Erosion Gully in an Open-Pit Coal Mine Dump During a Winter Freeze-Thaw Cycle by Using Low-Cost UAVs. *Remote Sensing*, *11*(11), 1356. https://doi.org/10.3390/rs11111356

Lague, D., Brodu, N., & Leroux, J. (2013). Accurate 3D comparison of complex topography with terrestrial laser scanner: Application to the Rangitikei canyon (N-Z). *ISPRS Journal of Photogrammetry and Remote Sensing*, *82*(February 2013), 10–26. https://doi.org/10.1016/j.isprsjprs.2013.04.009

Mancini, F., Dubbini, M., Gattelli, M., Stecchi, F., Fabbri, S., & Gabbianelli, G. (2013). Using Unmanned Aerial Vehicles (UAV) for High-Resolution Reconstruction of Topography: The Structure from Motion Approach on Coastal Environments. *Remote Sensing*, *5*(12), 6880–6898. https://doi.org/10.3390/rs5126880

Manconi, A., Ziegler, M., Blöchliger, T., & Wolter, A. (2019). Technical note: optimization of unmanned aerial vehicles flight planning in steep terrains. *International Journal of Remote Sensing*, *40*(7), 2483–2492. https://doi.org/10.1080/01431161.2019.1573334

Menegoni, N., Giordan, D., & Perotti, C. (2020). Reliability and uncertainties of the analysis of an unstable rock slope performed on RPAS digital outcrop models: The case of the gallivaggio landslide (Western Alps, Italy). *Remote Sensing*, *12*(10). https://doi.org/10.3390/rs12101635

Mourato, S., Fernandez, P., Pereira, L., & Moreira, M. (2017). Improving a DSM Obtained by Unmanned Aerial Vehicles for Flood Modelling. *IOP Conference Series: Earth and Environmental Science*, *95*(2). https://doi.org/10.1088/1755-1315/95/2/022014

Nesbit, P. R., & Hugenholtz, C. H. (2019). Enhancing UAV-SfM 3D model accuracy in high-relief landscapes by incorporating oblique images. *Remote Sensing*, *11*(3), 1–24. https://doi.org/10.3390/rs11030239

Pérez, M., Agüera, F., & Carvajal, F. (2011). Digital camera calibration using images taken from an unmanned aerial vehicle. *International Archives of the Photogrammetry, Remote Sensing and Spatial Information Sciences - ISPRS Archives*, *38*(1C22).

Rossi, G., Tanteri, L., Tofani, V., Vannocci, P., Moretti, S., & Casagli, N. (2018). Multitemporal UAV surveys for landslide mapping and characterization. *Landslides*, *15*(5), 1045–1052. https://doi.org/10.1007/s10346-018-0978-0

Westoby, M. J., Brasington, J., Glasser, N. F., Hambrey, M. J., & Reynolds, J. M. (2012). "Structure-from-Motion" photogrammetry: A low-cost, effective tool for geoscience applications. *Geomorphology*, *179*, 300–314. https://doi.org/10.1016/j.geomorph.2012.08.021